Manuscript accepted by Journal: Geology
DOI: 10.1130/G50429.1

Disparate crustal thicknesses beneath oceanic transform faults and adjacent fracture zones revealed by gravity anomalies

Zhikui Guo[1, 2], Sibiao Liu[2], Lars Rüpke[2, *], Ingo Grevemeyer[2], Jason P. Morgan[3], Dietrich Lange[2], Yu Ren[2] and Chunhui Tao[1, 4, *]

[1] *Key Laboratory of Submarine Geosciences, SOA, Second Institute of Oceanography, MNR, 310012 Hangzhou, China*

[2] *GEOMAR, Helmholtz Centre for Ocean Research, Wischhofstrasse 1-3, 24148 Kiel, Germany*

[3] *Southern University of Science and Technology, Xueyuan Avenue 1088, 518055 Shenzhen, China*

[4] *School of Oceanography, Shanghai Jiao Tong University, 1954 Huashan Rd., Shanghai 200030, China*

[*] lruepke@geomar.de, taochunhui@sio.org.cn

ABSTRACT

Plate tectonics describes oceanic transform faults as conservative strike-slip boundaries, where lithosphere is neither created nor destroyed. Therefore, seafloor accreted at ridge-transform intersections should follow a similar subsidence trend with age as lithosphere that forms away from ridge-transform intersections. Yet, recent compilations of high-resolution bathymetry show that the seafloor is significantly deeper along transform faults than it is at the adjacent fracture zones. We present residual mantle Bouguer anomalies, a proxy for crustal thickness, for 11 transform fault systems across the full range of spreading rates. Our results

DOI: 10.1130/G50429.1

indicate that the crust is thinner in the transform deformation zone than it is in either the adjacent fracture zones or the inside corner regions. Consequently, oceanic transform faulting appears not only to thin the transform valley crust but to also leads to a secondary phase of magmatic addition at the transition to the passive fracture zones. These observations challenge the concept of transform faults being conservative plate boundaries.

INTRODUCTION

Plate tectonics theory considers oceanic transform faults (TFs, Fig. 1A) to be conservative strike-slip plate boundaries that offset mid-ocean ridge (MOR, Fig. 1A) segments along small circles of plate motion (Morgan, 1968). Oceanic fracture zones (FZs, Fig. 1A), the passive extensions of active TFs, are visible as thousands-of-kilometers-long scars on the ocean floor. As lithosphere would be neither created nor destroyed in pure strike-slip motion, ocean plates sliding past one another along TFs should follow a similar age-dependent subsidence curve in response to plate cooling as does "normal" oceanic lithosphere away from ridge-transform intersections (RTIs, Fig. 1A) (Stein and Stein, 1992). Yet, thermal contraction induced by cooling of the oceanic lithosphere causes a horizontal shrinking component in plates (Turcotte, 1974; Kumar and Gordon, 2016), which can potentially lead to azimuths of transform faults that challenge the predictions that assume plates to be rigid (Mishra and Gordon, 2016). In addition, a recent systematic analysis of seafloor topography along TFs and FZs indicates that the topography of the TF is always deeper (up to 1.6 km) than its adjacent FZs (Grevemeyer et al., 2021). By combining bathymetric observations with 3-D geodynamic flow models, Grevemeyer et al. (2021) hypothesized that the deeper seafloor along the TF is linked to extension in the inside corner region (IC in Fig. 1A) of the RTI. The shoaling of the seafloor at the TF to FZ

DOI: 10.1130/G50429.1

transition may, in turn, be related to magmatic addition, a hypothesis that is corroborated by characteristic magmatic features such as J-shaped ridges and magmatic flows visible in bathymetric data. If correct, this evolution scenario implies that the crust along TFs is systematically thinner than that along their associated FZs. This corollary can be tested using residual mantle Bouguer gravity anomalies (RMBA) under the common assumption that they can be interpreted as a proxy for crustal thickness variations (Lin and Morgan, 1992). Previous gravity studies revealed that crustal accretion becomes asymmetric towards segment ends of slow-spreading ridges, with IC crust being systematically thinner than crust of the outside corner (OC, Fig. 1A; Escartin and Lin, 1995). Likewise, Gregg et al., (2007) found that the crust beneath slow-spreading ridge segments tends to be thicker than the crust beneath their connecting TF, while intermediate to fast-slipping TFs appear to have a mass deficit with respect to the adjacent ridge segment that may originate from having a thicker, more porous, and/or more altered transform crust.

The differences between the gravity signals of FZs and their connecting TFs where they were “born” have never been systematically explored. While the inference that transform faults could be non-conservative can be deduced from prior works (e.g., Turcotte, 1974; Mishra and Gordon, 2016; Sasajima and Ito, 2017), this hypothesis has rarely been explicitly proposed. Hence, more robust observational evidence is still needed to answer the first-order question of whether TFs are conservative strike-slip boundaries in a “classic” plate tectonics sense, or whether transform faulting itself modulates crustal thickness by tectono-magmatic processes in a non-conservative way. We address this question by integrating high-resolution multibeam bathymetry from 11 TFs (Fig. 1; Table S2 in the Supplement Material[1]), satellite gravity data, and 3-D geodynamic models to compute RMBA differences between the TF and their associated

FZs ($\Delta RMBA_{TF-FZ}$). Our analysis reveals systematically positive $\Delta RMBA_{TF-FZ}$ values, which suggests that tectonics and magmatism at the TF cause a disparity between crustal thicknesses beneath oceanic FZs and TFs.

DATA AND METHOD

We used RMBA as a proxy for crustal thickness variations following the method of Prince and Forsyth (1988). We first calculated the mantle Bouguer anomaly (MBA) from satellite free-air anomaly data (Sandwell et al., 2014) with Parker's method (Parker, 1973) using high-resolution multibeam bathymetric data in combination with the global ETOPO1 bathymetric dataset (NOAA National Geophysical Data Center, 2009) as needed to fill data gaps. After removing the gravitational effects of the water-crust and crust-Moho interface with an assumed 6 km normal crustal thickness, the MBA mainly reflects variations in crustal thickness and the thermally-induced density structure of the mantle. The RMBA is then determined by removing the thermally-induced mantle density effects from the MBA. The thermal correction is based on an accurate gravity forward method of a prism (Nagy, 1966) and temperature-induced density anomalies are estimated from 3-D geodynamic models following the approaches of Grevemeyer et al. (2021) and Behn et al. (2007). See Table S1 and Figs. S1 and S2 in the Supplemental Material for more detail. In contrast to MBA, RMBA is mainly caused by anomalous crustal thickness variations and/or mantle density effects that are not resolved by the thermal correction model.

To investigate RMBA changes between TF domains and their associated FZs, we define the mean difference $\Delta RMBA_{TF-FZ} = RMBA_{TF} - (RMBA_{FZ1} + RMBA_{FZ2})/2$ based on the approach proposed by Gregg et al. (2007), where $RMBA_{TF}$, $RMBA_{FZ1}$, and $RMBA_{FZ2}$ are mean RMBA values along the TF domain and the two associated fracture zones FZ1 and FZ2, respectively.

$RMBA_{TF}$ is calculated by averaging the values over a 10-km-wide rectangular box covering the TF (red box in Fig. 2). The length of the box is 90% of the TF length. At some places like the East Pacific Rise, where TFs are wider due to internal segmentation, we use separate boxes for each transform segment identified from bathymetric data (Fig. S13). $RMBA_{FZ1}$ and $RMBA_{FZ2}$ are calculated by averaging RMBA values in a 10-km-wide box that starts at the RTI and extends along the FZ. The box length depends on the coverage of the multibeam bathymetric data that characterize the FZ (blue boxes in Fig. 2). Note that resolution tests show that variations in box length affected the results by less than 5% (Fig. DR 16).

RESULTS

The 11 transform systems and their RMBA maps are shown in Fig. 1. The seafloor bathymetry, MBA, thermal correction, and RMBA map of each TF-FZ system are shown in Figs. DR3-13. Results indicate a correlation between the spreading rate and the RMBA value of a spreading segment, with positive anomalies at intermediate- and fast-spreading ridges and negative anomalies at slow- and ultraslow-spreading ridges. This feature (Fig. DR 15) results in a similar trend of the spreading rate versus RMBA difference between TF and the associated ridge segments as reported by Gregg et al. (2007).

Fig. 2 illustrates the workflow for computing the RMBA for the Atlantis TF. The bathymetry in Fig. 2A shows that the transform valley is deeper than its adjacent FZs. A positive RMBA anomaly centered around the transform valley suggests relatively thin crust in the transform deformation zone with respect to the FZs and MORs. This relative variation of crustal thickness (Fig. 2F) can be inverted from the RMBA map based on Parker-Oldenburg’s algorithm (Gómez-Ortiz and Bhrigu, 2005).

The systematic analysis of the $\Delta RMBA_{TF-FZ}$ shows that it is positive for almost all of the transform systems studied regardless of spreading rate (Fig. 3A). The vertical error bars refer to the RMBA variation between two FZs ($|RMBA_{FZ1}$- $RMBA_{FZ2}|$) of the transform system. The magnitude of $\Delta RMBA_{TF-FZ}$ appears to decrease with increasing spreading rate. It is interesting to note that the Atlantis II transform with the largest age offset (~30 m.y.) appears to have an anomalously low $\Delta RMBA_{TF-FZ}$, which could be caused by additional effects unrelated to crustal thickness variation, such as mantle serpentinization (~10%) and increased rock porosity (~10%) in the crust (Fig. DR 19). The geological and geophysical evidence seems to support thin crust (~ 2.7 km), and a highly fractured and serpentinized lower layer beneath the Atlantis II transform valley (Detrick et al., 1993; Muller et al., 2000), which implies that the crustal-thickness-related $\Delta RMBA_{TF-FZ}$ of Atlantis II could be closer to the overall trend.

DISCUSSION

The gravity field at ridge-TF-FZ systems reveals distinct and characteristic differences between the active TF domain, the adjacent FZs, and the ridge segments. Particularly striking are the systematically higher RMBA values in the transform domain with respect to the RMBA along the adjacent FZs. A key question is whether this is a consequence of transform faulting-related thermo-magmatic processes, or of the aforementioned asymmetry between IC and OC crust at MOR segment ends (Severinghaus and Macdonald, 1988; Escartin and Lin, 1995), in which case the $RMBA_{TF}$ should be close to $RMBA_{IC}$ and $RMBA_{FZ}$ and in between $RMBA_{IC}$ and $RMBA_{OC}$ with $0.5(RMBA_{IC} + RMBA_{OC})$ being a reasonable baseline. To discriminate, Fig. 3B shows the RMBA differences between IC and OC, and Fig. 3C the differences between $\Delta RMBA_{TF-FZ}$ and $0.5\Delta RMBA_{IC-OC}$. The latter is nearly always positive with values of up to 20

DOI: 10.1130/G50429.1

mGal. To test which crustal configurations are compatible with this observation, we performed synthetic tests with differing OC, IC, TF, and FZ crustal thicknesses (Fig. DR 17-18). Fig. 3D shows that the crust in the transform fault must also be thinner than IC crust on the order 0-1.5 km to make $\Delta RMBA_{TF-FZ} - 0.5\Delta RMBA_{IC-OC}$ positive.

Thin TF crust was previously proposed to explain the deep transform valley (e.g., Morgan and Forsyth, 1988). The thinner crust could result from perturbations in melt generation and migration caused by the lower upwelling rates near the transform and the depth of the permeability barrier at the base of the thermal boundary layer (Morgan and Forsyth, 1988; Gregg et al., 2009). Melt segregation and migration are controlled by the thermal structure of the lithosphere and magma budget along ridge segments (Morgan and Forsyth, 1988; Sparks and Parmentier, 1991), and these factors are spreading rate-dependent, i.e., the depth of the isothermal surface (e.g., 700°C) is deepening, and the magma supply is attenuating at slower spreading rates (Chen, 1988; Furlong et al., 2001).

We favor an alternative but complementary view in which the thin transform crust is the result of extension (Grevemeyer et al., 2021; Ren et al., 2022). In this scenario, the difference in plate strength (a consequence of the age offset) results in an increasingly oblique plate boundary at depth, which causes extension and mantle upwelling (Grevemeyer et al., 2021; Furlong et al., 2001). This proposed extension may therefore be an inherent feature of transform faulting and is consistent with extensional focal mechanisms observed along the Kane (Wilcock et al., 1990) and Oceanographer (Cessaro and Hussong, 1986) transforms on the Mid-Atlantic Ridge. Although gravity data alone cannot discriminate between the contributions of tectonic extension and lower melt supply to crustal thinning, it does suggest that the systematically positive, spreading rate-dependent RMBA along the active transform domain is plausibly due to crustal thinning whose relative importance tends to diminish as the spreading rate increases.

As the gravity data support relatively thicker crust beneath FZs than beneath their adjacent TF, we interpret the observed shoaling of the young FZ seafloor at RTIs (Grevemeyer et al., 2021) as being related to the magmatic addition and/or preferential asymmetric crustal accretion towards the OC. Evidence for thermal rejuvenation in combination with magmatic addition was first reported for the fast-slipping Clipperton transform (northern East Pacific Rise; Gallo et al., 1986; Barth et al. 1994) and recently, based on high-resolution bathymetric data, for transform systems of all spreading rates (Grevemeyer et al., 2021). A complementary view is that of "dueling" ridge tips that would occasionally propagate beyond the TF (Pollard and Aydin, 1984). In this view, magmatic addition would be more dynamic and unnecessary in a stable transform-to-fracture zone transition. Despite these uncertainties, the systematic trend in $\Delta RMBA_{TF\text{-}FZ}$ shown in Fig. 3A indicates that the magmatic addition is particularly pronounced at ultraslow to slow spreading rates.

The RMBA is typically interpreted in terms of crustal thickness variations. However, it cannot discriminate between additional density-changing processes such as variations in porosity, mantle serpentinization, and temperature states not resolved by the mantle flow model. When combined with other independent observations, the systematically positive $\Delta RMBA_{TF\text{-}FZ}$ in our results does point to thinner crust along the TF domains compared to their adjacent FZs. For ultraslow- to slow-spreading systems, crustal thinning and seafloor deepening in the TF domain have been inferred from geomorphology, gravity data, and seismic data (Fox et al., 1976; Muller et al., 2000). At fast-slipping TF systems, seismic studies indicate that the crust below the TF is slightly thinner than normal oceanic crust (Van Avendonk et al., 2001), and that it thickens beneath the FZ (Van Avendonk et al., 1998; Barth, 1994). This feature is consistent with the slightly positive RMBA in our study (Fig. 3 and Fig. S6). Furthermore, thin crust along transform domains correlates with the observed systematic deepening of transform valleys that is seen in the statistics of a recent compilation of 41 transform systems (Grevemeyer et al., 2021). Therefore, the observed positive $\Delta RMBA_{TF\text{-}FZ}$ could be induced by both crustal thinning along TFs and the thicker crust in their adjacent FZs that is being created when transform seafloor passes by the opposing ridge tip at the ridge-transform intersection. This oceanic transform-related mode of deformation and multi-stage accretion has significant implications for the composition and hydrothermal state of crust and lithosphere along FZs, material that has generally been inferred to represent altered and hydrated crust and mantle (Detrick et al., 1993). Instead, FZs may actually contain magmatically accreted crust (Marjanović et al., 2020; Growe et al., 2021) that has experienced two distinct phases of accretion and hydrothermal alteration at an active spreading center, which has implications for the possibility of systematic compositional and evolutionary differences between FZs and their adjacent oceanic lithosphere. Therefore, the fractured and hydrated lithosphere of oceanic transform faults will be magmatically overprinted by RTI magmatism, revealing the accretionary nature of oceanic transform faults and hence contradicting the idea that transform faults are conservative plate boundaries.

ACKNOWLEDGMENTS

We thank the National Natural Science Foundation of China (grant 42127807), the Scientific Research Fund of the Second Institute of Oceanography, Ministry of Natural Resources, China (grant SZ2201) and China Ocean Mineral Resources R&D Association (grant DY135-S1-01-01) for funding support, and Norddeutscher Verbund für Hoch- und

Höchstleistungsrechnen for parallel computing support. We thank the editor and the reviewers (Richard G Gordon, Mark Behn, and three anonymous reviewers) for their constructive comments, which helped to improve the manuscript.

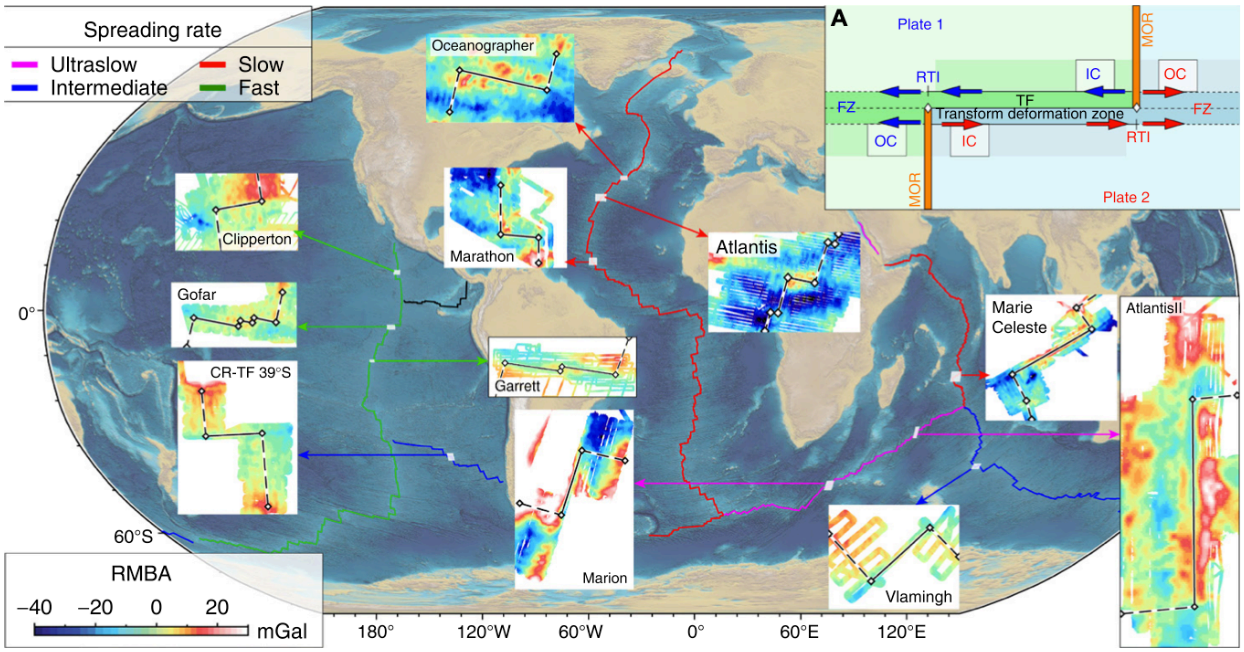

Figure 1. Global map of transform faults (TFs) included in this study and their residual mantle Bouguer anomaly (RMBA). Colors of the ridges represent different spreading rates (see legend). Dashed black lines are spreading ridge segments; solid black lines are TFs; diamonds are ridge-transform intersections (RTIs). CR-TF 39°S is the transform fault near 39°S offsetting the Chile Ridge. (A) Inset shows the basic geometry and magmatic-tectonic elements of a transform-fracture-zone system. FZ–fracture zone; OC–outside corner; IC–inside corner; MOR–mid ocean ridge.

DOI: 10.1130/G50429.1

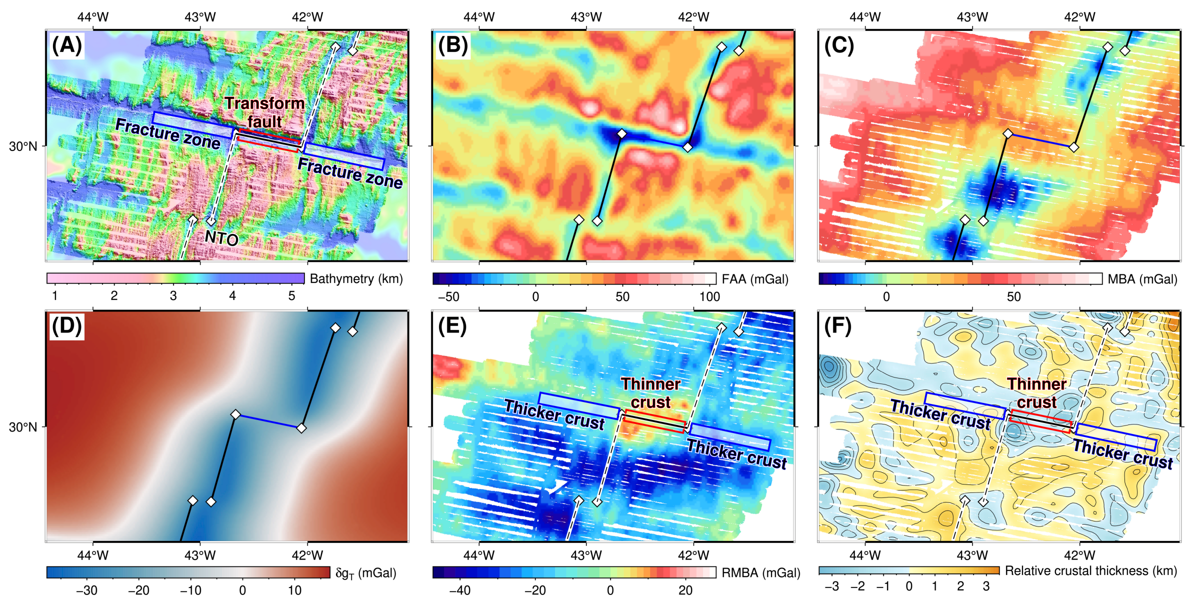

Figure 2. Results for the Atlantis transform on the Mid-Atlantic Ridge. (A) Seafloor topography merged from multibeam bathymetric data and ETOPO1 (NOAA National Geophysical Data Center, 2009). NTO–non-transform offset. The other symbols as Figure 1. (B) Free-air anomaly (FAA) derived from satellite. (C) Calculated mantle Bouguer anomaly (MBA). (D) Gravity anomaly of thermal contribution estimated from a 3-D viscoplastic mantle upwelling model. (E) Calculated residual mantle Bouguer anomaly (RMBA). (F) Map of gravity-derived relative variation of crustal thickness with contour 1 km. All gravity anomalies are relative to average value of TF zone (red box). Blue and red boxes indicate regions where mean RMBA values were calculated for the FZ and TF, respectively.

DOI: 10.1130/G50429.1

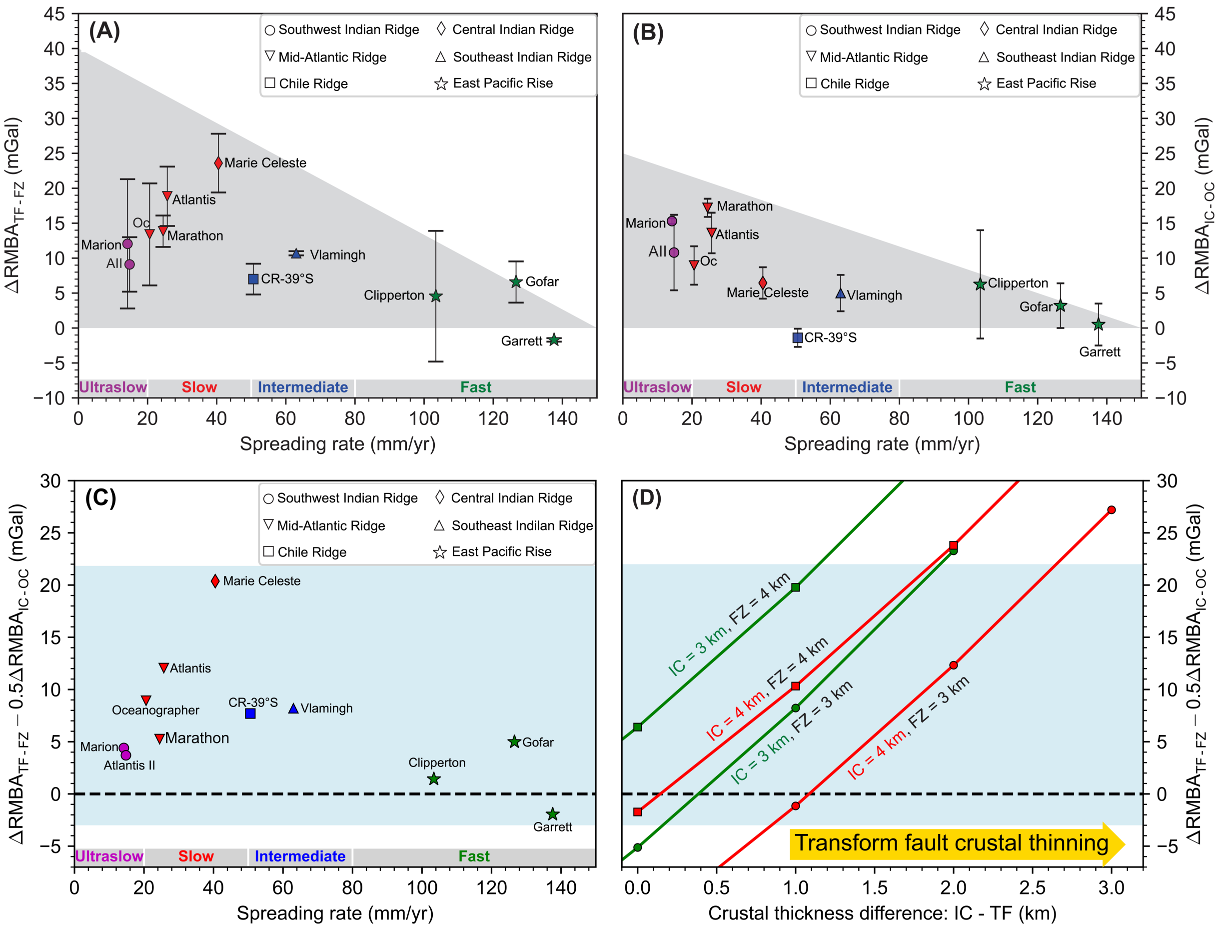

Figure 3. Gravity analysis result. Variation of $\Delta RMBA_{TF\text{-}FZ}$ (A) and $\Delta RMBA_{IC\text{-}OC}$ (B) as a function of spreading rate. TF–transform fault; FZ–fracture zone; OC–outside corner; IC–inside corner. (C) Difference between $\Delta RMBA_{TF\text{-}FZ}$ and $0.5\Delta RMBA_{IC\text{-}OC}$. Different symbols indicate the associated spreading ridges. AII–Atlantis II; Oc–Oceanographer. (D) Synthetic model result of $\Delta RMBA_{TF\text{-}FZ} - 0.5\Delta RMBA_{IC\text{-}OC}$ as a function of TF crust thinning relative to IC. The x-axis shows extra thinning of transform crust with respect to the IC, and the red and green lines show predictions of the synthetic models. The shaded-blue area is the observed range of differences between $\Delta RMBA_{TF\text{-}FZ}$ and $0.5\Delta RMBA_{IC\text{-}OC}$ that needs to be explained (red and green curves need to be in the shaded-blue region). The crustal thickness of the OC in this synthetic model

DOI: 10.1130/G50429.1

calculation is 5 km. Additional details of the theoretical model calculation and results with OC crust thickness 6 km and 7 km can be found in Fig. S17 and S18.

REFERENCES CITED

Barth, G., 1994, Oceanic crust thickens approaching the Clipperton Fracture Zone: Marine geophysical researches, v. 16, p. 51–64, https://doi.org/10.1007/BF01812445.

Behn, M. D., Boettcher, M. S., and Hirth, G., 2007, Thermal structure of oceanic transform faults: Geology, v. 35, p. 307–310, https://doi.org/10.1130/G23112A.1.

Cessaro, R.K., and D.M. Hussong, 1986, Transform seismicity at the intersection of the Oceanographer Fracture Zone and the Mid-Atlantic Ridge, Journal of Geophysical Research: Solid Earth, v. 91, p. 4839-4853, https://doi.org/10.1029/JB091iB05p04839.

Chen, Y., 1988, Thermal model of oceanic transform faults: Journal of Geophysical Research: Solid Earth, v. 93, p. 8839–8851, https://doi.org/10.1029/JB093iB08p08839.

Detrick, R., White, R., and Purdy, G., 1993, Crustal structure of North Atlantic fracture zones: Reviews of Geophysics, v. 31, p. 439–458, https://doi.org/10.1029/93RG01952.

Escartín, J. and Lin, J, 1995, Ridge offsets, normal faulting, and gravity anomalies of slow spreading ridges: Journal of Geophysical Research: Solid Earth, v. 100, p. 6163–6177, https://doi.org/10.1029/94JB03267.

Fox, P. J., Schreiber, E., Rowlett, H., and McCamy, K., 1976, The geology of the Oceanographer Fracture Zone: a model for fracture zones: Journal of Geophysical Research, v. 81, p. 4117–4128, https://doi.org/10.1029/JB081i023p04117.

Furlong, K. P., Sheaffer, S. D., and Malservisi, R., 2001, Thermal-rheological controls on deformation within oceanic transforms: Geological Society, London, Special

DOI: 10.1130/G50429.1

Publications, v. 186, p. 65–83, https://doi.org/10.1144/GSL.SP.2001.186.01.05.

Gallo, D.G., Fox, P.J., and Macdonald, K.C., 1986, A Sea Beam investigation of the Clipperton transform fault: The morphotectonic expression of a fast slipping transform boundary: Journal of Geophysical Research: Solid Earth, v. 91, p. 3455- 3467, https://doi.org/10.1029/JB091iB03p03455 .

Gómez-Ortiz, D., and Bhrigu NP A., 2005, 3DINVER. M: a MATLAB program to invert the gravity anomaly over a 3D horizontal density interface by Parker–Oldenburg's algorithm: Computers & geosciences, v. 31, p. 513-520, https://doi.org/10.1016/j.cageo.2004.11.004.

Gregg, P., Behn, M., Lin, J., and Grove, T., 2009, Melt generation, crystallization, and extraction beneath segmented oceanic transform faults: Journal of Geophysical Research: Solid Earth, v. 114, no. B11102, https://doi.org/10.1029/2008JB006100.

Gregg, P. M., Lin, J., Behn, M. D., and Montési, L. G., 2007, Spreading rate dependence of gravity anomalies along oceanic transform faults: Nature, v. 448, p. 183–187, https://doi.org/10.1038/nature05962.

Grevemeyer, I., Rüpke, L. H., Morgan, J. P., Iyer, K., and Devey, C. W., 2021, Extensional tectonics and two-stage crustal accretion at oceanic transform faults: Nature, v. 591, p. 402–407, https://doi.org/10.1038/s41586-021-03278-9.

Growe, K., Grevemeyer, I., Singh, S. C., Marjanović, M., Gregory, E. P., Papenberg, C., et al., 2021. Seismic structure of the St. Paul Fracture Zone and Late Cretaceous to Mid Eocene oceanic crust in the equatorial Atlantic Ocean near 18° W. Journal of Geophysical Research: Solid Earth, v. 126, e2021JB022456, https://doi.org/10.1029/2021JB022456.

Kumar, R. R. and Gordon, R. G., 2009, Horizontal thermal contraction of oceanic lithosphere:

Manuscript accepted by Journal: Geology
DOI: 10.1130/G50429.1

The ultimate limit to the rigid plate approximation: Journal of Geophysical Research: Solid Earth, v. 114, no. B01403. https://doi.org/10.1029/2007JB005473 .

Lin, J. and Morgan, J. P., 1992, The spreading rate dependence of three-dimensional mid-ocean ridge gravity structure: Geophysical Research Letters, v. 19, p. 13–16, https://doi.org/10.1029/91GL03041.

Marjanović, M., Singh, S. C., Gregory, E. P., Grevemeyer, I., Growe, K., Wang, Z., Vaddineni, V., Laurencin, M., Carton, H., Gómez de la Peña, L., et al., 2020, Seismic crustal structure and morphotectonic features associated with the Chain Fracture Zone and their role in the evolution of the equatorial Atlantic region: Journal of Geophysical Research: Solid Earth, v. 125, no. e2020JB020275, https://doi.org/10.1029/2020JB020275.

Mishra J. K. and Gordon, R. G., 2016, The rigid-plate and shrinking-plate hypotheses: Implications for the azimuths of transform faults: Tectonics, v. 35, p. 1827-1842. https://doi.org/10.1002/2015TC003968 .

Morgan, J. P. and Forsyth, D. W., 1988, Three-dimensional flow and temperature perturbations due to a transform offset: Effects on oceanic crustal and upper mantle structure: Journal of Geophysical Research: Solid Earth, v. 93, p. 2955–2966, https://doi.org/10.1029/JB093iB04p02955.

Morgan, W. J., 1968, Rises, trenches, great faults, and crustal blocks: Journal of Geophysical Research: Solid Earth, v. 73, p. 1959–1982, https://doi.org/10.1029/jb073i006p01959.

Muller, M. R., Minshull, T. A., and White, R., 2000, Crustal structure of the Southwest Indian Ridge at the Atlantis II fracture zone: Journal of Geophysical Research: Solid Earth, v. 105, p. 25809–25828, https://doi.org/10.1029/2000JB900262.

Nagy, D., 1966, The gravitational attraction of a right rectangular prism: Geophysics, v. 31, p.

362–371, https://doi.org/10.1190/1.1439779.

NOAA National Geophysical Data Center, 2009: ETOPO1 1 Arc-Minute Global Relief Model: NOAA National Centers for Environmental Information, https://doi.org/10.7289/V5C8276M.

Parker, R., 1973, The rapid calculation of potential anomalies: Geophysical Journal International, v. 31, p. 447–455, https://doi.org/10.1111/j.1365-246X.1973.tb06513.x.

Pollard, D. D., and Aydin, A., 1984, Propagation and linkage of oceanic ridge segments. Journal of Geophysical Research: Solid Earth, v. 89, p. 10017–10028, https://doi.org/10.1029/JB089iB12p10017.

Prince, R. A. and Forsyth, D. W., 1988, Horizontal extent of anomalously thin crust near the Vema Fracture Zone from the three-dimensional analysis of gravity anomalies: Journal of Geophysical Research: Solid Earth, v. 93, p. 8051–8097, https://doi.org/10.1029/JB093iB07p08051.

Ren, Y., Geersen, J., and Grevemeyer, I., 2022, Impact of spreading rate and age-offset on oceanic transform fault morphology: Geophysical Research Letters, v. 49, p. 1-10, https://doi.org/10.1029/2021GL096170.

Sandwell, D. T., Müller, R. D., Smith, W. H., Garcia, E., and Francis, R., 2014, New global marine gravity model fromCryoSat-2 and Jason-1 reveals buried tectonic structure: Science, v. 346, p. 65–67, https://doi.org/10.1126/science.1258213.

Sasajima R. and Ito T., 2017, Anisotropic horizontal thermal contraction of young oceanic lithosphere inferred from stress release due to oceanic intraplate earthquakes: Tectonics, v. 36, p. 1988-2021. https://doi.org/10.1002/2017TC004680 .

Severinghaus, J. P. and Macdonald, K. C, 1988, High inside corners at ridge-transform intersections: Marine Geophysical Research, v. 9, p. 353–367, https://doi.org/10.1007/BF00315005.

Sparks, D. W. and Parmentier, E. M., 1991, Melt extraction from the mantle beneath spreading centers: Earth and Planetary Science Letters, v. 105, p. 368–377, https://doi.org/10.1016/0012-821X(91)90178-K.

Stein, C. A., and Stein, S., 1992, A model for the global variation in oceanic depth and heat flow with lithospheric age: Nature, v. 359, p. 123–129, https://doi.org/10.1038/359123a0.

Turcotte D L., 1974, Are transform faults thermal contraction cracks?: Journal of Geophysical Research, v. 79, p. 2573-2577, https://doi.org/10.1029/JB079i017p02573.

Van Avendonk, H., Harding, A., Orcutt, J., and McClain, J., 2001, Contrast in crustal structure across the Clipperton transform fault from travel time tomography: Journal of Geophysical Research: Solid Earth, v. 106, p. 10961–10981, https://doi.org/10.1029/2000JB900459.

Van Avendonk, H. J., Harding, A. J., Orcutt, J. A., and McClain, J. S., 1998, A two-dimensional tomographic study of the Clipperton transform fault: Journal of Geophysical Research: Solid Earth, v. 103, p. 17885–17899, https://doi.org/10.1029/98JB00904.

Wilcock, W. S., Purdy, G., and Solomon, S. C., 1990, Microearthquake evidence for extension across the Kane transform fault: Journal of Geophysical Research: Solid Earth, v. 95, p. 15439–15462, https://doi.org/10.1029/JB095iB10p15439.

[1]GSA Data Repository item 201Xxxx, details on the geodynamic model, thermal correction and additional results of all 11 transform faults, is available online at www.geosociety.org/pubs/ft20XX.htm, or on request from editing@geosociety.org.